Space Sci Rev (2011) 160:95–121
DOI 10.1007/s11214-011-9820-x

Properties of Near-Earth Magnetic Reconnection from In-Situ Observations

S.A. Fuselier · W.S. Lewis

Received: 11 May 2011 / Accepted: 5 August 2011 / Published online: 24 September 2011

Abstract Many properties of magnetic reconnection have been determined from in-situ spacecraft observations in the Earth's magnetosphere. Recent studies have focused on ion scale lengths and have largely confirmed theoretical predictions. In addition, some interesting features of reconnection regions on electron scale lengths have been identified. These recent studies have demonstrated the need for combined plasma and field measurements on electron scale lengths in the reconnection diffusion regions at the magnetopause and in the magnetotail. They have also indicated that measurements, such as those that will be made by the Magnetospheric Multiscale mission in the near future, will have a significant impact on understanding magnetic reconnection as a fundamental plasma process.

Keywords Magnetic reconnection · Magnetosphere · Magnetospheric multiscale · Plasma physics

1 Reconnection in the Near-Earth Environment

Magnetic reconnection occurs between two separate magnetized plasmas across a thin current sheet, creating an interconnection between the two plasmas. Traditionally, magnetic reconnection has been associated with three regions of Earth's magnetosphere: at the dayside magnetopause, on the nightside in the near-Earth magnetotail, and in the distant magnetotail. Figure 1 illustrates schematically the occurrence of reconnection at the dayside magnetopause and in the near-Earth tail under conditions of southward interplanetary magnetic field (IMF). (The reconnection site in the distant tail is not shown.) On the dayside, reconnection occurs between draped solar wind field lines in the magnetosheath (shown in blue) and closed geomagnetic field lines (shown in green), forming an "X-line" at the

S.A. Fuselier (✉)
Lockheed Martin Advanced Technology Center, Palo Alto, CA, USA
e-mail: stephen.a.fuselier@lmco.com

W.S. Lewis
Southwest Research Institute, San Antonio, TX, USA

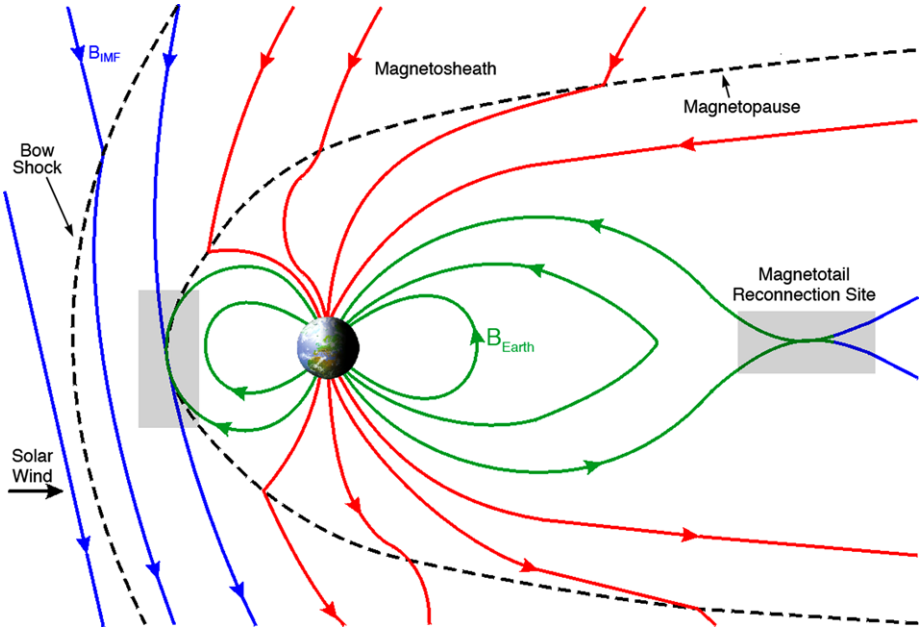

Fig. 1 Some near-Earth regions where reconnection occurs. Solar wind field lines (*blue*) cross the bow shock and interact with magnetospheric field lines (*green*) on the dayside. In the *grey box*, the field lines reconnect, producing open field lines (*red*). The *open field lines* are transported antisunward by the solar wind flow and form the lobes of the magnetotail. The accumulation of magnetic flux in the lobes ultimately becomes unsustainable, leading to reconnection in the near-Earth tail (*grey box*), first of closed plasma sheet field lines and then of the *open field lines* in the lobes. Figure adapted from W.J. Hughes, The magnetopause, magnetotail, and magnetic reconnection, in Introduction to Space Physics, ed. by M.G. Kivelson, C.T. Russell (Cambridge University Press, Cambridge, UK, 1995), p. 243

thin magnetopause current sheet (inside the grey box). The oppositely oriented solar wind and geomagnetic field lines "break" and then "reconnect" with one another in a small region where the plasma becomes demagnetized, creating "open" field lines (in red) extending from the Earth into the solar wind (and ultimately back to the Sun). (Although the idea of breaking field lines is commonly and traditionally (e.g., Dungey 1953) used in conceptual descriptions of magnetic reconnection, it should be noted that it is, strictly speaking, physically incorrect and represents merely a convenient shorthand for a complex topological reconfiguration.) Convective motion of the solar wind transfers magnetic flux and plasma from the dayside to the nightside, eroding the dayside magnetosphere and building up magnetic flux in the tail. As flux builds up, Earth's magnetic field lines on the nightside stretch and a thin current sheet forms in the near-Earth magnetotail (between 20 and 30 Earth radii, R_E, from the Earth). A second reconnection X-line forms periodically across this current sheet (inside the grey box in the magnetotail). This reconnection expels flux in the form of magnetically closed or, more likely, flux rope (twisted magnetic field) structures known as plasmoids out of the Earth's magnetotail. The tail reconnection process also accelerates plasma earthward into the near-Earth environment, and creates closed field lines (in green) on the nightside. In this conceptual picture of reconnection, the important aspects of the process are the reconfiguration or change in magnetic topology of the magnetic field lines and the fact that this topological change occurs in very small regions at the magnetopause and in the magnetotail.

The process of dayside and nightside reconnection just described was first proposed by Dungey (1961). Since then, important details have been filled in, including dependency on external solar wind conditions, time dependency, and near-continuous presence of a distant X-line. However, the basic picture of flux transport into and out of the magnetosphere and of the circulation of plasma within the magnetosphere driven by reconnection remains unchanged since it was first introduced.

Figure 1 presents a simplified 2-dimensional representation of the reconnection process at the subsolar magnetopause and in the near-Earth tail. In reality, reconnection occurs in three dimensions, at varying locations depending on solar wind conditions and time and sometimes simultaneously at multiple locations within a general reconnection region, on a variety of spatial scales, and in bursty as well as quasi-continuous fashion. It is well known, for example, that where reconnection occurs on the dayside depends on IMF orientation: mainly at high latitudes on the magnetopause when the IMF is northward and at lower latitudes when the IMF is southward. Further, it is well known that the initiation of near-Earth reconnection in the tail depends on time history of the IMF and that this reconnection region moves tailward and may change orientation as it moves.

Finally, although the scope of the present article is limited to the terrestrial magnetosphere, it should be noted that in-situ observations have provided evidence for the occurrence of magnetic reconnection in other planetary magnetospheres. Magnetic field and plasma/particle data from the Pioneer, Voyager, Galileo, and Cassini missions indicate that reconnection occurs both at the magnetopause and in the tail of the rotationally driven magnetospheres of Jupiter (e.g., Russell and Walker 1985; Russell et al. 1988; Kronberg et al. 2005; Vogt et al. 2010) and Saturn (e.g., Jackman et al. 2008; McAndrews et al. 2008). However, in the case of both giant planets, and in contrast to Earth, it has yet to be established to what extent magnetotail reconnection is driven externally (e.g., by dayside reconnection with the solar wind field) or internally (e.g., through the centrifugally driven stretching of mass-loaded flux tubes on the nightside) (cf. Kivelson and Southwood 2005; Badman and Cowley 2007). Reconnection has also been shown to occur at Mercury (Russell and Walker 1985; Slavin et al. 2009). Analysis of recent MESSENGER data has identified several reconnection-related phenomena in Mercury's tiny magnetosphere and determined a magnetopause reconnection rate that may be $\sim$10 times faster than that at Earth (Slavin et al. 2009). Recent studies have also revealed that reconnection occurs in the solar wind itself, far from any planetary magnetospheric boundary. Using data from variety of spacecraft, including Helios, Wind, ACE, Ulysses, and STEREO, numerous examples of reconnection events have been identified in solar wind current sheets over heliocentric distances from 0.3 to beyond 5 AU and with x-lines of several hundred R_E in extent (e.g., Gosling et al. 2005, 2006a, 2006b; Phan et al. 2006).

2 In-Situ Observations of Magnetic Reconnection

Initial predictions of reconnection in the near-Earth environment awaited direct confirmation from spacecraft observations. Large-scale plasma convection, correlation between magnetotail and magnetospheric activity (e.g., substorms) and IMF orientation, and observations of solar wind plasma within the Earth's magnetosphere were considered early, indirect evidence of reconnection. Other, more direct evidence included observations of a non-zero magnetic field component normal to the magnetopause (Sonnerup and Cahill 1967). Non-zero normal magnetic fields demonstrate connection between magnetosheath and magnetospheric magnetic fields across the magnetopause current layer. In basic reconnection theory, the magnitude of the normal component is related to the reconnection rate.

Direct verification of reconnection on a more local scale required relatively high-time resolution measurements of both plasma and field structures at the magnetopause and in the magnetotail. The twin-spacecraft International Sun Earth Explorer (ISEE) mission provided plasma instrumentation with appropriate time resolution as well as the ability to distinguish between spatial and temporal phenomena using two-spacecraft observations. Initial in-situ measurements (e.g., Russell and Elphic 1978, 1979; Paschmann et al. 1979; Sonnerup et al. 1981) produced strong evidence for the occurrence of reconnection at the magnetopause and also indicated that it could be localized in space and intermittent in time (in the form of so-called flux transfer events or FTEs; see the discussion of reconnection variability in Sect. 5). Similarly, early evidence for the occurrence of reconnection in the magnetotail was provided by in-situ measurements by the Vela and IMP satellites in the plasma sheet (e.g., Hones 1976; Frank et al. 1976).

Evidence of reconnection included observations of high-speed flows or jets of plasma emanating from reconnection sites (Hones 1976; Paschmann et al. 1979). Jets of plasma result from conversion of magnetic energy to particle energy (a fundamental process in reconnection). According to reconnection theory (e.g., Vasyliunas 1975), the outflow velocity is related to the local Alfvén speed, a prediction that initial observations confirmed. The high-speed flows were evidence that, as in the case of solar flares, reconnection in the magnetosphere occurs much more rapidly than predicted by the Sweet-Parker model (Sweet 1958; Parker 1963) and were interpreted in terms of the Petschek model (Petschek 1964) of fast reconnection (Hones 1976; Paschmann et al. 1979).

The Vela, IMP, and ISEE results were followed by important observations of many other aspects of reconnection that have confirmed predictions and/or encouraged new theory and simulations. Over the ensuing 30+ years, reconnection has been firmly established as the primary transport mechanism for mass and energy across the magnetopause and the dominant process in reconfiguration of the Earth's magnetotail. It has been established as a fundamental process for conversion of magnetic energy to particle energy in many other plasma environments as well. Many books, chapters in books, and review articles describing in-situ observations of reconnection have been published during the past three decades (e.g., Hones 1984; Song et al. 1995; Hultqvist and Øieroset 1997; Hultqvist et al. 1999; Paschmann 2008; Burch and Drake 2009). Rather than repeating or updating much of what has been reviewed already, the present paper reviews more recent in-situ observations of several important aspects of magnetic reconnection and places particular emphasis on multispacecraft results that have direct implications for NASA's future 4-spacecraft Magnetospheric Multiscale (MMS) mission (scheduled for launch in 2014). This review is organized around three aspects of reconnection that are subject to recent investigations using in-situ measurements: reconnection scale lengths (Sect. 3), reconnection topology (Sect. 4), and reconnection rates (Sect. 5). After these aspects are discussed, the MMS mission is introduced (Sect. 6). The discussion section (Sect. 7) then summarizes the aspects of reconnection covered in Sects. 3 through 5 and discusses these aspects in connection with the MMS mission.

3 Reconnection Scale Lengths

Theory and modeling have established scale lengths for several phenomena associated with reconnection, as illustrated in Fig. 2, which shows a cross section of the reconnection region from a simulation with a guide field (e.g., Hesse 2006). The guide field is the non-zero component of the total magnetic field and exists because the shear across the reconnecting current sheet is not exactly 180°. The simulation assumes equal plasma densities and magnetic field strengths on both sides of the current sheet (symmetric reconnection). The guide

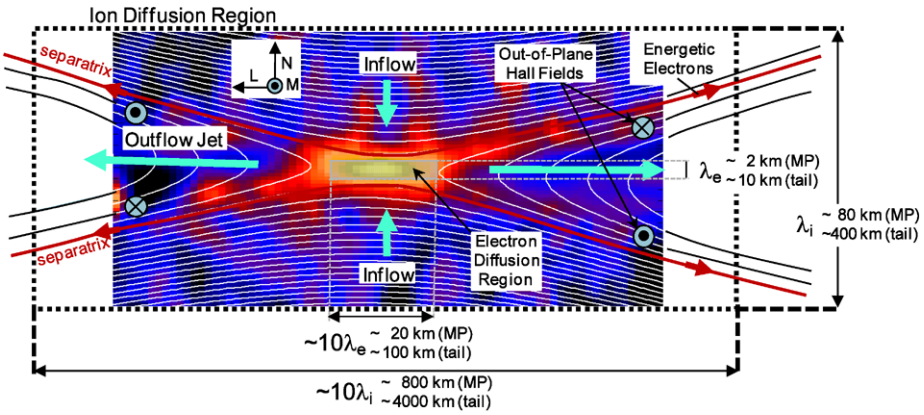

Fig. 2 Some phenomena and scale lengths of ion and electron reconnection diffusion regions. The background is from a guide field simulation and shows the parallel electric field, which is high in the electron diffusion region. Estimated thicknesses and widths of electron and ion diffusion regions are shown in skin depths (λ) and km for typical conditions at the magnetopause (MP) and in the magnetotail (tail). An aspect ratio of 0.1 is assumed. (See text for a discussion of recent simulation results indicating a larger "two-scale" electron diffusion region.) Plasma and magnetic field inflows symmetrically from the top and bottom and are accelerated in out the two sides. Other features include out-of-plane Hall fields and energetic electrons flowing along the separatrices

magnetic field is directed out of the plane of the figure, parallel to the current. The lines denote magnetic fields and the background color indicates the magnitude of the parallel electric field (with blue low and yellow/white high). For direct comparison with observations, it is convenient to use a boundary normal (LMN) coordinate system as defined in the upper left of Fig. 2. The maximum change in the magnetic field occurs across the current sheet in the L direction. The N direction is normal to the current sheet, and the M direction is along the reconnection line, which is often called the x-line. Plasma flows into the reconnection region at equal rates from the top and bottom (parallel and anti-parallel to the N direction) and "jets" of plasma on reconnected field lines flow out of the left and right sides (parallel and anti-parallel to the L direction).

The region of strong parallel electric field in the center of Fig. 2 is the electron diffusion region, where electrons become demagnetized and magnetic fields on either side of the current sheet (viewed edge-on and running through the center of the figure) reconnect. This small region is embedded in the much larger ion diffusion region, where ions become demagnetized. The electron and ion diffusion regions have a thickness in the N direction, a width in the L direction, and a length in the M direction (into and out of the plane of the figure). Theory and simulations (e.g., Hesse 2006) have demonstrated that the thicknesses and widths of the ion and electron diffusion regions are determined by three quantities: (1) the plasma density near the electron diffusion region, (2) the rate at which plasma inflows into the diffusion region (i.e., the reconnection rate), and (3) the ion to electron mass ratio. The dimensions of the diffusion regions shown in Fig. 2 follow from the choice of plasma density and reconnection rate and the assumption that the plasma is dominated by protons. Two different values for each dimension are given, one for average conditions at the magnetopause (MP) and one for average conditions in the near-Earth magnetotail.

The thickness of the electron diffusion region is approximately the electron skin depth, $\lambda_e = c/\omega_{pe}$), which is proportional to $1/\sqrt{n_e}$ (Hesse 2006). At the magnetopause, this scale length is $\sim$2 km for a density near the diffusion region of 10 cm^{-3} (i.e., for a reconnection

layer density that is half of an average magnetosheath density of 20 cm^{-3}). In the near-Earth magnetotail, the thickness is larger by about a factor of 5 because the average density in the vicinity of the near-Earth diffusion region is only about 0.3 cm^{-3} (Baumjohann 1993). Most reconnection simulations also show that the thickness of the ion diffusion region is $\sim\lambda_i = c/\omega_{pi}$, so that widths and thicknesses of the electron and ion diffusion regions are related by the square root of the mass ratio, which is approximately 43 for proton-dominated plasmas in the magnetosheath and magnetotail.

In fast reconnection, the reconnection rate is proportional to the thickness of the diffusion region divided by its width: the larger the aspect ratio, the faster the reconnection rate and vice versa. The dimensions illustrated in Fig. 2 are for an assumed reconnection rate of 0.1: $V_n/V_A = 0.1$, where V_n is the normal inflow velocity into the reconnection region and V_A is the local Alfvén speed (e.g., Shay et al. 1999). As discussed further below, however, recent simulations indicate that the dimensions of the diffusion region may be much larger than previously assumed and shown in the figure.

Figure 2 illustrates some of the observable phenomena associated with the electron and ion diffusion regions. Outflow jets constitute an important identifiable characteristic of reconnection and are observed very far away (thousands of kilometers) from the diffusion region. Such jets consist of ions and electrons accelerated to the local Alfvén speed in the plasma (when viewed in the deHoffman-Teller frame (deHoffmann and Teller 1950), where electric fields are zero everywhere except in the electron diffusion region). Associated with the outflow jets is a non-zero normal component to the magnetic field across the current layer. As noted above, ISEE observations of non-zero B_n at the magnetopause and comparison of plasma jet velocities measured by ISEE with the basic theory of reconnected current sheets constituted the first confirmation of the occurrence of reconnection at the magnetopause (Paschmann et al. 1979).

Other phenomena associated with the ion (and electron) diffusion region include a set of narrow separatrices that divide inflowing magnetic field lines from reconnected magnetic fields and out-of-plane components to the magnetic field in the ion diffusion region. In the case of symmetric reconnection, out-of-plane magnetic fields form a characteristic quadrupolar pattern within the ion diffusion region (Fig. 2). These out-of-plane, or Hall, fields become important on scale sizes of the order of the ion skin depth (Vasyliunas 1975). They are produced by a current system that results from the separation of demagnetized ions and still frozen-in electrons in the ion diffusion region (e.g., Sonnerup 1979; Hesse et al. 2001). The Hall currents are carried by field-aligned electrons flowing along the separatrices both toward and away from the x-line (Fujimoto et al. 1997; Nagai et al. 2003; Manapat et al. 2006).

The Hall current system and the quadrupolar magnetic field have been observed near or within reconnection regions in the magnetotail by Geotail (Nagai et al. 2001; Deng et al. 2004), Wind (Øieroset et al. 2001), Polar (Mozer et al. 2002), and Cluster (Runov et al. 2003; Borg et al. 2005; Eastwood et al. 2007, 2010). The quadrupolar structure of the out-of-plane field is clearly evident, for example, in magnetic field measurements made simultaneously on both sides of the current sheet by Cluster (Fig. 3) (Eastwood et al. 2010). While the symmetric reconnection model is appropriate for the magnetotail, where plasma densities and field strengths on either side of the current sheet are comparable, densities and field strengths on either side of the dayside magnetopause are typically quite different. Analysis of data from magnetopause crossings by THEMIS spacecraft has shown that the quadrupolar field and bipolar electric field present in symmetric reconnection become bipolar and unipolar, respectively on the dayside, consistent with predictions from simulations of asymmetric reconnection (Mozer et al. 2008a, 2008b; Mozer and Pritchett 2011).

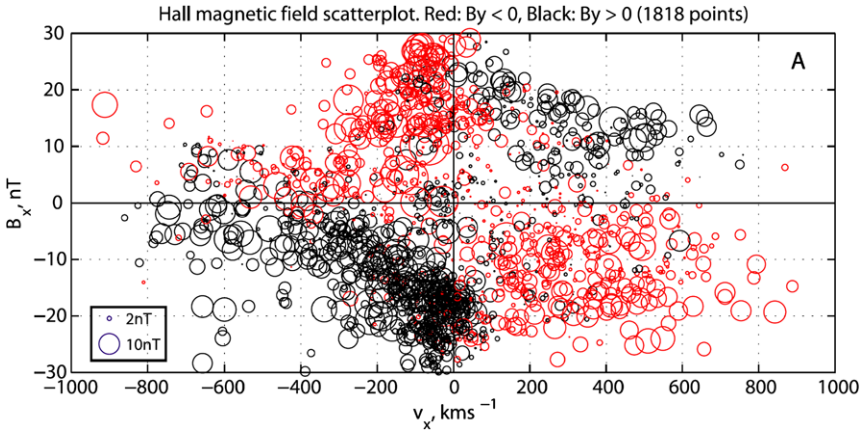

Fig. 3 Quadrupolar magnetic field observed by Cluster during encounters with diffusion regions in the magnetotail. The magnitude of the out-of-plane (B_y) field is indicated by the size of the *circles* (cf. the reference *circles in the lower left*). *Black* (*red*) denotes positive (negative) B_y. From Eastwood et al. (2010)

Recent numerical simulations (Daughton et al. 2006; Karimabadi et al. 2007; Shay et al. 2007; Drake et al. 2008; Klimas et al. 2008) have shown that the electron diffusion region can extend significantly farther in the L direction than illustrated in Fig. 2, and Cluster observations in the tail have confirmed the existence of the predicted elongated electron current sheet (Phan et al. 2007; Chen 2009). The elongated electron diffusion region in the simulations consists of an inner dissipation region, a few (0.6–5) λ_i in extent, and an outer region, 10s λ_i in extent, where a small fraction of electrons form a narrow outflow jet flowing much faster than the local Alfvén speed (Karimabadi et al. 2007; Shay et al. 2007). Based on the results of a 2.5-D particle-in-cell simulation, Klimas et al. (2008) concluded that it is the inner region, with an aspect ratio of ∼0.25, that controls the reconnection rate or "adjusts its geometry for compatibility with a rate that is set elsewhere, as in the Hall reconnection model."

Daughton et al. (2006) suggested that the development of the elongated electron diffusion region would slow the rate of reconnection, requiring the formation of secondary magnetic islands that break the extended diffusion region into shorter segments in order to sustain fast reconnection. Magnetic islands have been observed in association with the elongated electron current layer by Chen (2009). Other simulations have shown that, even with an elongated diffusion region, fast reconnection (with rates of ∼0.12) can proceed without the formation of secondary islands (Shay et al. 2007) and that the super-Alfvénic outflow jet is embedded in a broader expanding electron outflow that allows fast reconnection to occur (Shay et al. 2007; Drake et al. 2008). These simulation results are consistent with recent Cluster observations by Phan et al. (2007) of an elongated electron diffusion region with a super-Alfvénic jet extending ∼60λ_i from the x-line and embedded within a broader near-Alfvénic and frozen-in electron outflow; the calculated reconnection rate for this event is 0.07–0.09, consistent with the "canonical" rate of ∼0.1 for fast reconnection.

Simulations also show that Hall fields can extend well beyond the ion diffusion region. In fact, simulations (Drake et al. 2009) show Hall fields following separatrices out to many times the ion diffusion region width (and essentially to the limits of the simulation box). These fields occur at large distances because ions crossing the narrow separatrix boundary become unmagnetized, leading to the development of the out-of-plane fields.

The final characteristic scale length (not illustrated in Fig. 2) is the length of the reconnection line (along the M direction into and out of the plane in Fig. 2). Observations (e.g., Phan et al. 2000; Fuselier et al. 2002) show that the x-line is considerably longer than it is thick or wide. At the magnetopause, the total length depends on whether the magnetic fields on either side of the reconnecting current layer are exactly opposite one another (antiparallel reconnection) or whether a guide-field is present (component reconnection, defined as magnetic fields on either side of the current layer that have any orientation except anti-parallel). (Antiparallel and component reconnection are discussed further in Sect. 4.) Although the total length depends on the type of reconnection, for both types, dayside reconnection lines are inferred to be many Earth radii ($R_E = 6378$ km) long, or many thousands of times the width of the diffusion region. In the magnetotail, the reconnection line is also believed to be many R_E long and, in fact, is often inferred to stretch across the entire tail. Since the reconnection line is much longer than its width or thickness, to a good approximation, reconnection anywhere along the line can be reduced to the geometry illustrated in Fig. 2 (i.e., the end effects of the termination of a reconnection line can be ignored).

3.1 Diffusion Region Width and Thickness from In-Situ Observations

The diffusion region thickness is determined experimentally by timing spacecraft motion through the region. Typically, a spacecraft moves slowly (∼1 km/s) in its orbit compared to the average radial motion of the magnetopause (∼20 km/s, Phan and Paschmann 1996) or vertical motion of magnetotail, which may occur on velocity scales of the order of 10's of km/s. Thus, a spacecraft does not fly through a diffusion region. Rather the region passes over the nearly stationary spacecraft. At a magnetopause speed of 20 km/s, an electron diffusion region with scale length shown in Fig. 2 passes over the spacecraft in 0.1 s. This rapid motion of a thin structure over the spacecraft imposes an important, fundamental limitation on the use of state-of-the-art plasma instrumentation to investigate properties of the electron diffusion region. Although electric and magnetic field instruments on spacecraft such as Cluster (Gustafsson et al. 1993; Balogh et al. 1993) make measurements at a cadence of many samples per second, 3-D ion and electron measurements from these spacecraft are tied to the spacecraft spin rate (typically several seconds). Thus, plasma measurements are too slow to identify the electron diffusion region, much less probe the region and determine its properties and thickness. Although field and limited plasma observations within electron diffusion regions have been reported (e.g., Scudder et al. 2002; Mozer et al. 2003; Mozer 2005), much of the current observational research focuses on properties of the ion diffusion region, where time resolution of ion and electron instrumentation is sufficient.

As an example of ion diffusion region observations, Øieroset et al. (2001) reported on a direct encounter with an ion diffusion region in the magnetotail by the Wind spacecraft. Figure 4 illustrates the diffusion region and the Wind trajectory schematically, while Fig. 5 presents measurements of the ion density, ion velocity, and magnetic field components obtained as the spacecraft traversed the diffusion region. (Both figures are from Øieroset et al. 2001.) In the Cartesian coordinate system in Fig. 4, X is towards Earth and corresponds to the direction across the width of the diffusion region, Y is the direction along the reconnection line, and Z is the direction normal to the (reconnecting) magnetotail current sheet. In Fig. 5, the trajectory across the entire diffusion region is recognized in the reversal of V_x as the spacecraft first encounters an earthward flowing jet and then a tailward flowing jet. The Hall magnetic field structure is highlighted in the B_y panel, first in the reduction of the average B_y field (orange shading) and then in the increase (blue shading). The Hall fields are not symmetric about zero because of the presence of a guide field in the diffusion region.

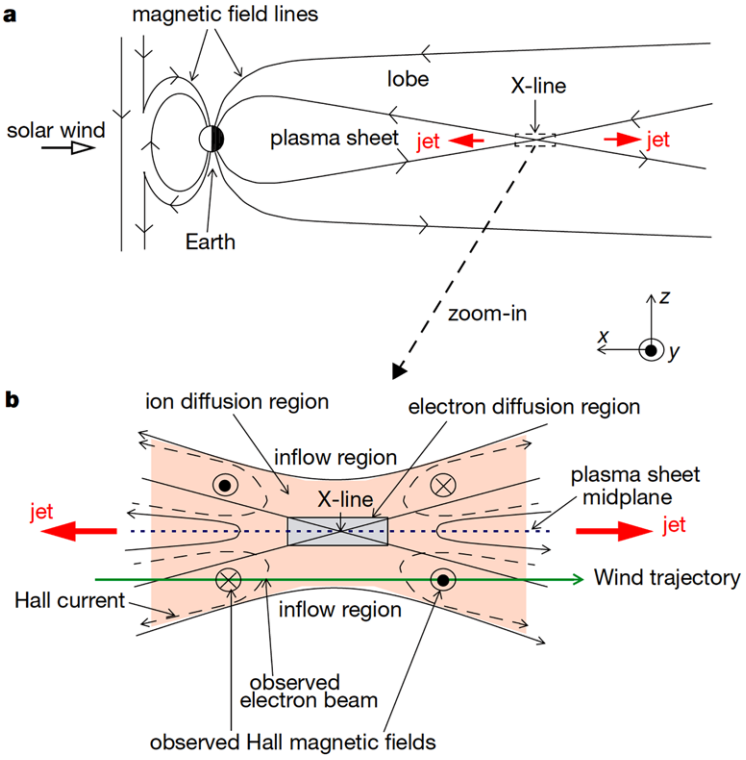

Fig. 4 (*Top*) Reconnection geometry in the magnetotail where bi-directional reconnection jets were observed. (*Bottom*) Blow-up of the reconnection region showing the spacecraft trajectory through the ion diffusion region, including the observed Hall magnetic fields. Reprinted by permission from Macmillan Publishers Ltd: [Nature] M. Øieroset et al., In situ detection of collisionless reconnection in Earth's magnetotail, Nature, 412, 414, copyright 2001

For example, the asymmetrical structure of the parallel electric field in Fig. 2, results from the presence of the guide field in the simulation.

Because this encounter involved only a single spacecraft, the only way to estimate the size of the diffusion region is to determine the duration of the encounter and to assume that the reconnection x-line was stationary with the spacecraft moving through it at its known velocity of ∼1 km/s. Using this assumption, Øieroset et al. (2001) estimate that the ion diffusion region width was 1300 km or about $2\lambda_i$. The actual width depends on motion of the reconnection line relative to the spacecraft during the encounter (which could be nearly zero or much larger than the spacecraft motion), motion relative to the normal direction (i.e., the spacecraft could move into or out of the diffusion region simply by vertical motion of the entire reconnection line), and diffusion region thickness and reconnection rate at the time of the encounter (quantities that are also unknown).

Nagai et al. (2010) approached the single spacecraft limitation in a similar manner for another magnetotail reconnection event, but used the difference in the tailward and sunward flow velocities to estimate the speed of the x-line past the Geotail spacecraft and therefore the size of the ion diffusion region. For this event, they report an ion diffusion region width of $\sim 8\lambda_i$. The Øieroset et al. (2001) and Nagai et al. (2010) studies illustrate the difficulties in determining fundamental properties of diffusion regions from single spacecraft observa-

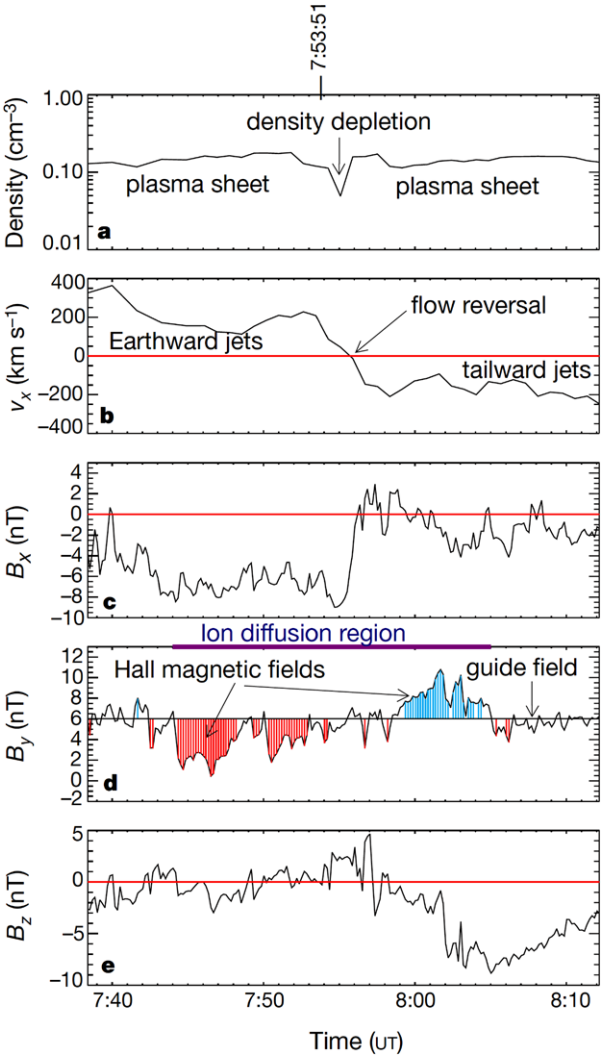

Fig. 5 Observations of an ion diffusion region in the tail. (Top to bottom) Plasma density, earthward-tailward flow velocity, three components of the magnetic field. As the spacecraft passed through the ion diffusion region, out-of-plane Hall fields were observed. This magnetotail reconnection event had a substantial guide field. Reprinted by permission from Macmillan Publishers Ltd: [Nature] M. Øieroset et al., In situ detection of collisionless reconnection in Earth's magnetotail, Nature, 412, 414, copyright 2001

tions, but they also demonstrate that ion diffusion region widths derived from spacecraft observations are in reasonable agreement with theoretical predictions.

Multispacecraft observations provide more information on the thickness and width of the diffusion region, but suffer from some important limitations as well. The following discussion draws on the analysis by Zhang et al. (2008) of an encounter with the ion diffusion region on the dayside magnetopause by the Cluster spacecraft. Figure 6 (from Zhang et al. 2008) shows 12 minutes of plasma and magnetic field data from the encounter, during which the spacecraft traverse the ion diffusion region on a trajectory more-or-less perpendicular to the magnetopause (i.e., in the N direction in Fig. 2). From top to bottom the panels in Fig. 6 show the ion density, L component of the ion velocity, and LMN magnetic field components. During the 12-minute interval, the Cluster spacecraft move from the magnetosphere, through the magnetopause current layer (between the vertical dashed lines), and into the

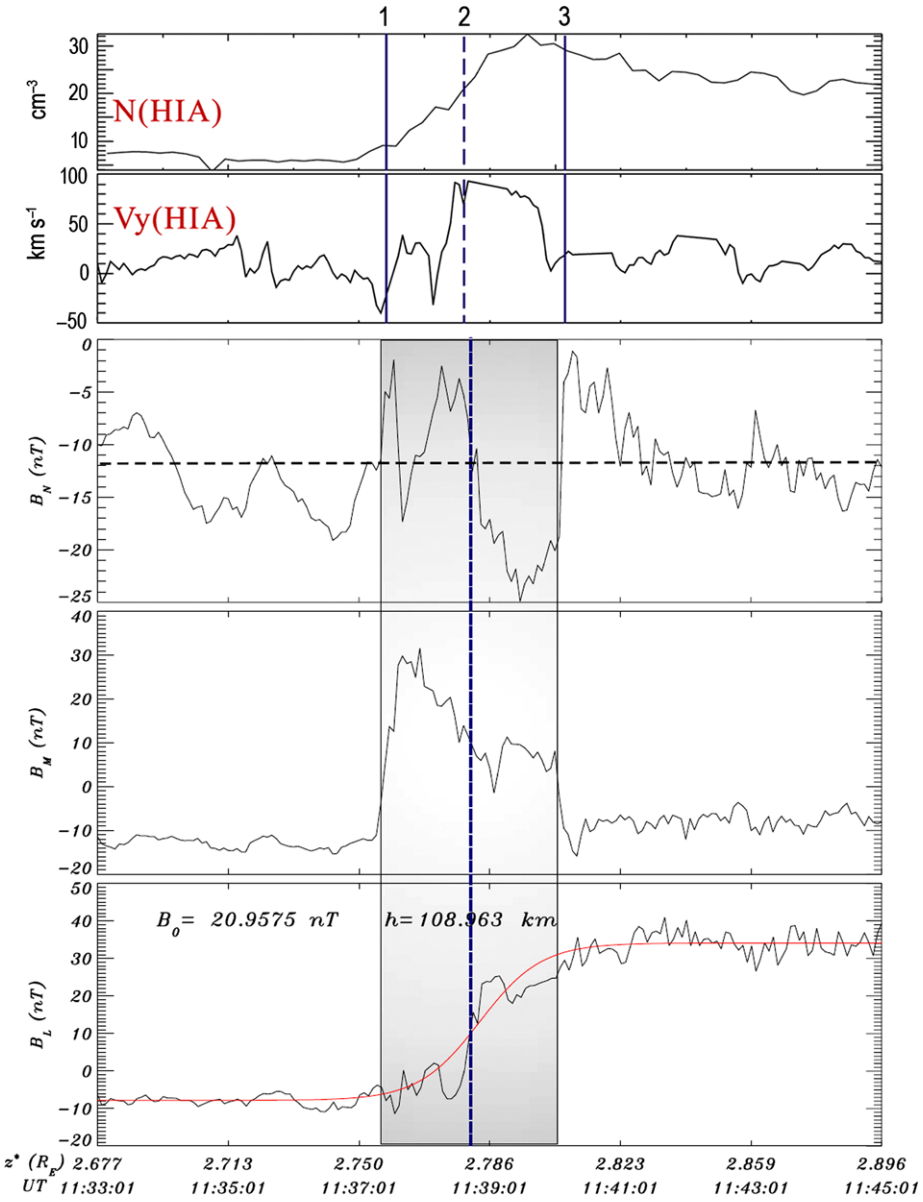

Fig. 6 Observations of Hall fields at the magnetopause. (Top to bottom) Plasma density, L velocity, and LMN magnetic field components. As the spacecraft crosses the magnetopause from the magnetosphere *on the left* to the magnetosheath *on the right*, a reconnection jet in the L direction is observed. Associated with this jet is a unipolar Hall magnetic field in the B_M direction. The Hall field is in one direction only because the reconnection is asymmetric with magnetic field dominating the pressure in the magnetosphere and the plasma dominating the pressure in the magnetosheath. Modified from Zhang et al. (2008)

magnetosheath. A density gradient across the magnetopause compresses the ion diffusion region on the magnetosheath side. The high velocity in the L direction in the current layer identifies the reconnection jet flowing away from the inner diffusion region. The deviation

of the magnetic field M component from its value in the magnetosheath and magnetosphere is evidence of the Hall magnetic field in the current layer. Just as in the magnetotail case discussed above, the M component is not zero on either side of the current layer because there is a guide field in the reconnection region.

During the current layer crossing, the four Cluster spacecraft were separated by ∼100 km. From the spacecraft separations and the differences in the times when the spacecraft encounter the magnetopause current layer, Zhang et al. (2008) could compute the speed of the current layer and translate the time taken to cross it into a distance approximately normal to the layer. The distance thus calculated is 218 km, or, given the average density in the current layer, about 5–6λ_i. The computed thickness is somewhat larger than λ_i. The actual trajectory of the spacecraft through the current layer is not known, but it was most likely not exactly along the normal direction. The computed thickness of the ion diffusion region is therefore an upper limit on the actual thickness.

Since the spacecraft were separated in the L–M direction as well as in the N direction and all four spacecraft observed nearly the same diffusion region structure (Zhang et al. 2008), it was possible to determine at least a minimum width for the ion diffusion region. The maximum separation of the spacecraft in the L direction (perpendicular to the reconnection line in the M direction) was only about 100 km, yielding an estimated minimum width of ∼2.5λ_i for the diffusion region. Because the distance from the spacecraft to the reconnection line is not known, only a minimum width can be calculated. Some studies (e.g., Phan et al. 2007) use additional information and/or simulations to estimate this distance and have calculated sizes for the ion diffusion region consistent with the scale sizes illustrated in Fig. 2. However, all of these studies suffer from the basic limitation that exact spacecraft trajectories through the diffusion region and distances to the reconnection line are not known. Therefore only upper limits on the thickness of the ion diffusion region and lower limits on its width can be determined.

3.2 Separatrices

The separatrices (Fig. 2) divide magnetic fields with different topologies. Simulations show that there are thin, electron scale layers associated with these separatrices that extend far beyond the electron diffusion region (André et al. 2004; Vaivads et al. 2006). Figure 7 (from André et al. 2004) shows electron phenomena associated with a Cluster spacecraft crossing of one of these layers. Plotted from top to bottom are the electron flux perpendicular and parallel to the magnetic field, derived quantities of the electric field (E), the Hall term of the generalized Ohm's law ($(1/n_e)\mathbf{j} \times \mathbf{B}$, where n_e is the electron density, $\mathbf{j}$ is the current and $\mathbf{B}$ is the magnetic field), the pressure gradient of the generalized Ohm's law, $T_e\, dn/dx$, where T_e is the electron temperature), and the current parallel and perpendicular to the magnetic field. Only 2.5 seconds of data are shown from a much longer transition of the magnetopause current layer. Since the spin rate for the spacecraft is 4 seconds, a full electron distribution is not obtained in the narrow layer in the center of the figure, which has a duration of only 0.2 seconds. Nonetheless, enhancements in field-aligned electrons between 100 eV and 1 keV in the second panel of Fig. 7 are seen in the narrow layer. Higher time resolution electric and magnetic field measurements combined with assumptions about the electron density (from lower time resolution electron measurements) are used to estimate important quantities (like the Hall term of Ohm's law) related to these energetic electrons. These field-aligned electrons are the current carriers for the field-aligned current shown in the bottom panel. The agreement between $\mathbf{E}$ and $(1/n_e)\mathbf{j} \times \mathbf{B}$ in the third panel indicates that the electrons are magnetized and drifting relative to the fixed ion background.

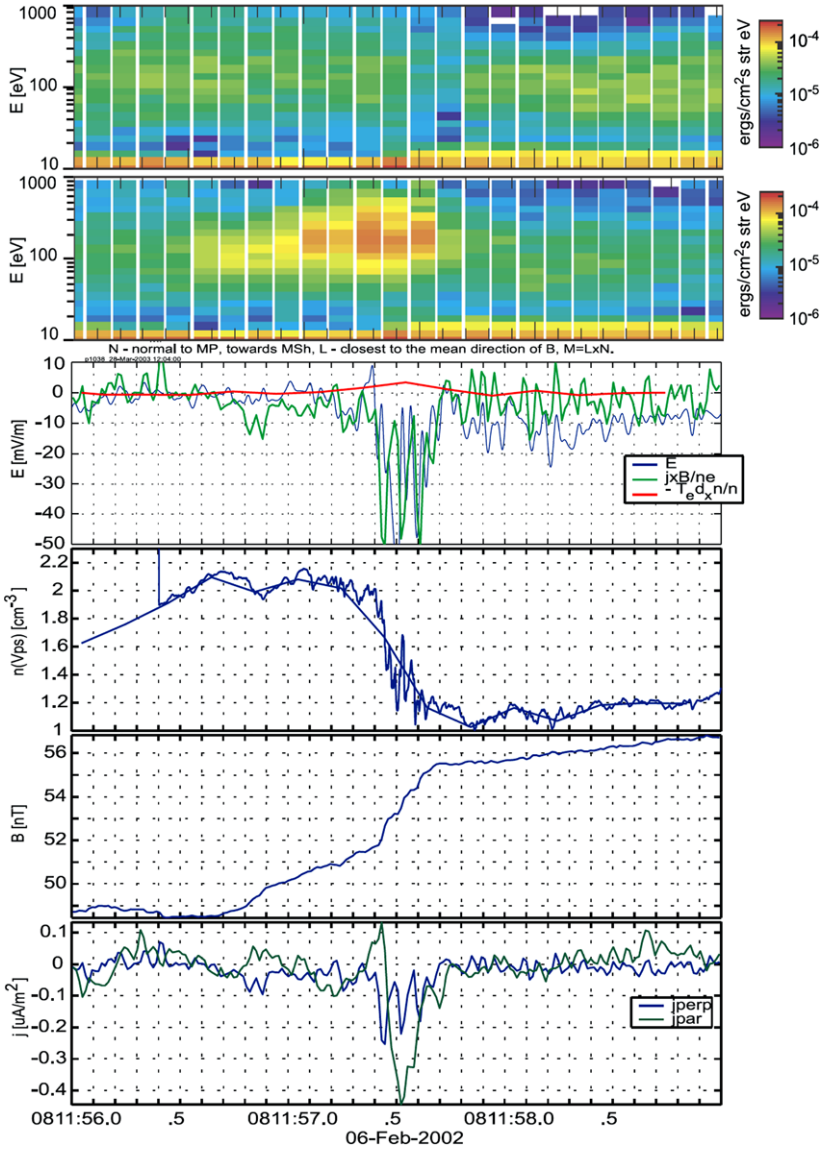

Fig. 7 Top to bottom: electron flux perpendicular and parallel to the magnetic field, Hall term and pressure gradient of the generalized Ohm's law, $T_e\, dn/dx$, and the current parallel and perpendicular to the magnetic field. Enhancements in field aligned electrons are seen in a narrow layer. These electrons are the current carriers for the field-aligned current in the *bottom panel*. The agreement between $\mathbf{E}$ and $1/n_e\mathbf{j} \times \mathbf{B}$ in the *third panel* indicates that the electrons are magnetized and drifting relative to a fixed ion background. From André et al. (2004)

The electron beam in Fig. 7 is observed at some distance from the reconnection site. Similar to other observations discussed in this section, the exact distance is not determined because the location of the reconnection site relative to the spacecraft location is not known.

What is known about these electrons at the separatrices is that they have a profound effect on the region around the separatrices. Large amplitude solitary waves have been identified in encounters of separatrices in the magnetotail (Cattell et al. 2005). The waves are the result of growth and collapse of electron holes (regions of depleted electron density and enhanced ion density) that are created by the turbulence driven by the intense electron beams. Simulations of these electron structures and their associated strong electric fields agree well with observations (Drake et al. 2003). These results suggest that the birth and death of electron holes leads to strong electron scattering and energization. Furthermore, the narrow electron structures extend back to the electron diffusion region, providing a window into that region and allowing investigation of diffusion region properties (albeit modified greatly by strong wave-particle interactions along the separatrices) from a vantage point well removed from the actual region where electrons are demagnetized.

4 Location of Reconnection Sites

Magnetic reconnection is believed to occur somewhere at the magnetopause for any IMF orientation, with the type of reconnection being defined in terms of the shear angle between the IMF/magnetosheath field and Earth's magnetic field (e.g., Trattner et al. 2007a, 2007b). Reconnection that occurs only where the shear is ∼180° and the magnetopause currents are largest is termed antiparallel reconnection. In contrast, component reconnection (equivalent to guide-field reconnection in computer simulations) occurs at locations where magnetosheath and magnetospheric field lines are not strictly antiparallel. Driven by the convection of magnetosheath magnetic fields against the magnetopause (with shears as low as 50°), component reconnection occurs at the subsolar point and along a line hinged at this point and extending around the flanks of the magnetosphere. The particular model for component reconnection is often described as the tilted neutral line model because of the tilted orientation of the reconnection line relative to the equatorial plane intersection of the subsolar magnetopause.

Observations demonstrate that both types of reconnection occur at the magnetopause. Usually, the location of the reconnection site is unknown, but the general direction of the site is determined from the direction of flow jets observed by a spacecraft crossing the magnetopause. Numerous statistical studies have used observed jet directions to demonstrate that reconnection occurs along a tilted reconnection line or at antiparallel sites on the magnetopause (e.g., Trenchi et al. 2008). On rare occasions, spacecraft observe jets that reverse direction as the spacecraft crosses the magnetopause (e.g., Phan et al. 2003; Retinò et al. 2005). Under these conditions, the shear between the magnetosheath and magnetospheric magnetic fields can be measured directly and the type of reconnection directly determined. However, such conditions occur rarely and, until now, the question of which type of reconnection dominated for specific solar wind conditions has remained unanswered.

The location of reconnection lines as a function of solar wind conditions can be determined by using observations in Earth's magnetospheric cusps. Solar wind ions crossing the open magnetopause follow field lines down to low altitudes in the cusps. The cusp field lines (shown in red in Fig. 1) convect tailward under the motion of the solar wind. The ions mirror at low altitudes and propagate back along field lines into the magnetotail. At a particular point in the cusp, the slowest ions to reach the spacecraft come from the reconnection site. The velocity difference between the slowest ions from the reconnection site and the

slowest ions to return to the spacecraft from the low altitude mirror point is proportional to the distance from the spacecraft to the reconnection site divided by the distance from the spacecraft to the mirror point at low altitudes. Using this velocity difference and a model magnetic field, one can calculate the distance from the spacecraft to the reconnection site (e.g., Onsager et al. 1991; Fuselier et al. 2002). As the spacecraft traverses the cusp in both latitude and longitude, distances along the magnetopause are determined, effectively mapping a reconnection line across a wide swath of the magnetopause.

Using the method just described and plasma data from 130 cusp crossings by the Polar spacecraft, Trattner et al. (2007a, 2007b) have mapped locations of reconnection sites on the magnetopause under a variety of IMF conditions and for different seasons. B_z was negative (southward) in all events, while the values for B_x and B_y ranged from positive to negative. Representative results from their study are illustrated in Fig. 8, in which reconnection lines derived from two Polar cusp crossings are mapped onto two-dimensional plots of the shear angle between model magnetosheath and magnetospheric field lines at the magnetopause.

For southward IMF ($B_z < 0$), antiparallel reconnection was found to be favored at the flanks of the magnetosphere for all B_y and B_z conditions. Antiparallel reconnection is also favored when B_x is large ($|B_x|/|B| > 0.7$) (Fig. 8, right panel) and when the clock angle of the IMF ($\arctan(B_y/B_z)$) is within 15° of due south. For other clock angles, component reconnection occurs along a tilted reconnection line that follows the maximum shear angle (black line in Fig. 8) across the dayside low latitude magnetopause and connects the antiparallel reconnection regions on the flanks (Fig. 8, left panel). Also, when the clock angle is within 15° of due south, the antiparallel reconnection line is continuous from the magnetopause flanks up to the noon meridian, but bifurcates across this meridian, as can be seen in both panels of Fig. 8. Observations of precipitating protons in the cusp (e.g., Fuselier et al. 2002; Petrinec and Fuselier 2003; Trattner et al. 2010) are consistent with the bifurcation. There is strong indication from a variety of observations (e.g., Phan et al. 2000; Fuselier et al. 2002) that the reconnection line is continuous for many Earth radii.

The position of the tilted reconnection line depends on the season (i.e., on the dipole tilt). For northern hemisphere summer (Fig. 8, left panel), the reconnection line crosses the noon meridian (often several R_E) south of the subsolar point ($Y_{GSM} = Z_{GSM} = 0$). For northern hemisphere winter (Fig. 8, right panel), the reconnection line lies north of the subsolar point. For fall and spring equinoxes, the reconnection line crosses at the subsolar point.

In the magnetotail, the location of reconnection sites and the type of reconnection are less well defined. Statistical studies show that near-Earth reconnection occurs between 20 and 30 R_E from the Earth (Nagai 2006) and in the distant tail approximately 100 R_E from the Earth. It is commonly assumed that antiparallel reconnection is dominant in the magnetotail. However, the guide field in Fig. 5 (from Øieroset et al. 2001) clearly indicates that component reconnection also occurs in the distant tail. The formation of electron holes at the separatrices in reconnection in the near-Earth magnetotail appears to require a guide field (Cattell et al. 2005; Drake et al. 2003). Nakamura et al. (2008) also present evidence of a guide field in a near-Earth magnetotail reconnection event In addition, Eastwood et al. (2010) have recently published a study based on simultaneous Cluster measurements of the Hall magnetic field perturbation above and below diffusion region current sheet in the near-Earth tail. While the majority of their cases were consistent with the expected pattern of anti-parallel reconnection, Eastwood et al. also demonstrate the distortion of the Hall electric and magnetic fields by a moderate guide field for some of their cases. The Eastwood et al. (2010) study is the closest one to a statistical study of the type of reconnection in the tail and it demonstrates the occurrence of both anti-parallel and component reconnection.

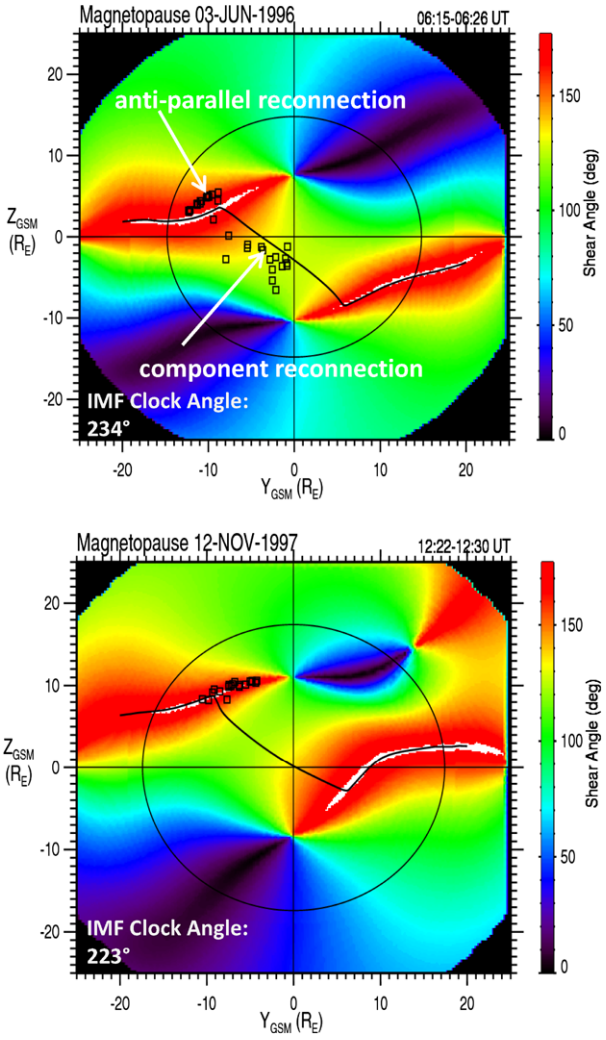

Fig. 8 Observed reconnection locations (*squares*) mapped onto plots of the modeled magnetic shear at the magnetopause. *Red* represents regions of high shear, where antiparallel reconnection is expected, while *blue* represents low shear (near 0°). The *black circle* shows the terminator ($X = 0$), separating the day side from the night side. The *white lines through the red regions* indicate locations where the shear between the magnetosheath and magnetospheric magnetic fields is 180° ± 3°. The *black line* running across the dayside and connecting the two antiparallel reconnection regions follows the maximum shear angle and represents the tilted (component) reconnection line. Values for the IMF components for the *panel on the top* are (−0.4, −2.4, −1.7) nT and for the *panel on the bottom* are (−2.4, −1.5, −0.9) nT. From Trattner et al. (2007a)

Like the magnetopause observations, statistical studies of the location and type of reconnection in the tail are limited because in-situ observations of flow jet reversals (cf. Fig. 5 from Øieroset et al. 2001) are the only way to determine unambiguously the location of the reconnection site and the orientation of the magnetic fields on either side of the reconnecting current sheet.

5 Reconnection Rates and Variability

5.1 Reconnection Rates

Magnetic reconnection proceeds at a rate that depends on the inflow speed of the plasma into the reconnection site. In Fig. 2, that inflow occurs in the ±N direction, and is denoted by V_n. Since the outflow jet velocity (in the ±L direction) is V_A, the Alfvén speed, the reconnection

rate is usually defined by the dimensionless quantity V_n/V_A. This simplified rate assumes there is no guide field (i.e., antiparallel reconnection) and assumes symmetric reconnection where the densities on either side of the reconnecting current sheet are the same. Also, this quantity is not a measure of the energy conversion rate (Mozer and Hull 2010). Significant complications are introduced when there is a guide field or, in asymmetric reconnection, when there is a density gradient across the current layer (e.g., Cassak and Shay 2007, 2008). However, setting these complications aside, the fast reconnection rate at the magnetopause and in the magnetotail is typically quoted to be $V_n/V_A \sim 0.1$ (e.g., Levy et al. 1964).

At the magnetopause and in the magnetotail, B_n/B, is proportional to V_n/V_A, where B_n is the magnetic field normal to the current layer. Measurement of non-zero B_n was one of the first verifications of reconnection at the magnetopause and, for a few cases when B_n was measured (e.g., Sonnerup et al. 1981; Phan et al. 2001), B_n/B was ∼0.1 to 0.2. However, measuring a normal component that is of the order of 10% of the total field requires knowledge of boundary normals to an accuracy better than a few degrees. Fluctuations in observed field strengths and directions across the magnetopause typically result in uncertainties in the normal to the current layer that are larger than a several degrees. Multispacecraft observations improve normal determinations, but the accuracy still remains no better than a few degrees (Haaland et al. 2004).

Direct measure of the inflow velocity V_n, is even more difficult than measuring B_n. Measuring V_n directly still requires knowledge of the magnetopause normal to within a few degrees. Normals are usually determined from magnetic field measurements, so the same issues with the accuracy of B_n apply. In addition, the magnetopause is almost always in motion, with velocities of ∼20 km/s (Phan and Paschmann 1996). Since the Alfvén speed is of the order of 200–300 km/s, the magnetopause velocity is of the same order as V_n. A spacecraft crossing the magnetopause measures the combined velocities of the magnetopause and V_n. Therefore, direct measure of V_n has additional uncertainties associated with separating two small, nearly equal velocities.

Another way to estimate the inflow velocity is to determine the tangential electric field, E_t, at the magnetopause. Similar to direct determination of V_n, measuring the tangential electric field requires determining the boundary normal and transforming it into a frame of reference where the magnetopause is stationary. Thus, determining the tangential electric field has the same uncertainties associated with the direct determination of V_n.

The same accuracy issues exist in spacecraft data from magnetotail current sheet crossings. Since reconnection rates in the tail are not expected to be larger than that at the magnetopause, normals to the magnetotail must be determined within a few degrees to use B_n/B, as a measure of the reconnection rate. The magnetotail motion is similar in magnitude to that of the magnetopause, so the same accuracy issues apply in the magnetotail for determining V_n or E_t.

Newer techniques either bypass these accuracy requirements (e.g., Fuselier et al. 2005), or reduce measurement error by estimating errors on small quantities such as E_t or B_n using larger magnitude components such as the electric field normal to the magnetopause or the magnetic field tangent to the magnetopause (e.g., Haaland et al. 2004; Mozer and Retinò 2007).

Figure 9 is a compilation of several reconnection rate measurements at the magnetopause using a variety of methods (including, Phan et al. 2001; Mozer et al. 2002; Fuselier et al. 2005, 2010; Mozer and Retinò 2007, and Vaivads et al. 2004). Plotted is the dimensionless rate V_n/V_A versus shear angle at the reconnection site. This plot should not be considered a statistical sampling of reconnection rates at the magnetopause. Given difficulties in determining rates, there is a strong bias in the literature towards high reconnection rates. Nonetheless, there are a few measurements of reconnection rates that are significantly smaller than

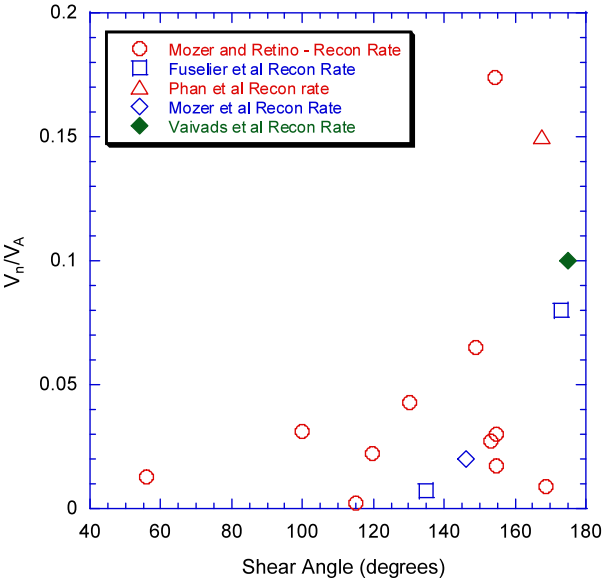

Fig. 9 V_n/V_A versus shear angle for several reconnection observations at the magnetopause. V_n/V_A is approximately the reconnection rate. The reconnection rate is small for low shear angle and increases as the shear angle approaches 180°

the canonical $V_n/V_A \sim 0.1$. These small reconnection rates tend to occur at smaller shear angles, leading to the conclusion that reconnection rate is proportional to shear angle at the magnetopause.

Theory (Pritchett 2001; Hesse et al. 2004) also predicts a reconnection rate that is proportional to shear angle (or, equivalently, magnitude of the guide field). However, theory predicts a much smaller change in the reconnection rate (only about 30%) over the range of shear angles in Fig. 9. Although there are large uncertainties in reconnection rates from spacecraft observations, the differences between the results shown in Fig. 9 and current theory are not explained. One possible explanation is that reconnection rate for large density shear across the current layer (a condition that often occurs at the magnetopause) depends on plasma beta and shear angle. In fact, simulations show that asymmetric reconnection for high beta and small shear is suppressed (Swisdak et al. 2003). Furthermore, it is not straightforward to associate V_n/V_A in Fig. 9 with reconnection rates for shear angles other than 180°. Thus, while there may be a discrepancy between observations and theory, much more work on the observations is needed to determine how large and statistically significant any discrepancy might be.

5.2 Variability

Thus far, there has been little mention of variability in reconnection. Reconnection in the near-Earth tail (between 20 and 30 R_E from the Earth) is highly variable. It is known that reconnection does not occur in the near-Earth tail for long periods of time. Then, at some point, reconnection starts and grows explosively (often in association with a substorm). After some period, the reconnection line either moves down the tail or reconnection stops and conditions return to a quiescent state. When discussing reconnection variability, the focus here is on driven reconnection at the dayside magnetopause.

For driven reconnection at a thin current sheet like the dayside magnetopause, one scenario is that reconnection is always occurring somewhere on the magnetopause. As discussed in Sect. 4, this reconnection location may move around in response to external con-

ditions, but, in this scenario, reconnection never ceases. A somewhat less modified scenario is that reconnection rates vary at the magnetopause, but never go to zero. Such variability would cause the thickness of the reconnection layer to vary with time, but would not change the characteristics of the reconnection jets. Indeed, a common interpretation of flux transfer events (FTEs) at the magnetopause, which goes back to their discovery, is that the reconnection rate at the magnetopause is variable in at least time, if not in time and space (Russell and Elphic 1978; Scholer 1988; Southwood et al. 1988).

The interpretation of FTEs as bulges on the magnetopause due to a change in the reconnection rate has been largely confirmed. Recent multi-spacecraft observations of FTEs (Owen et al. 2008) demonstrate that observed internal features (or layers) of an FTE depend simply on how deep the spacecraft penetrates into the bulge as it moves past. Although there is general agreement that FTEs are a product of variability in reconnection, it is not clear that the reconnection rate goes to zero between passes through FTEs. The only circumstantial evidence that the rate does not go to zero is that, when multiple spacecraft are located near one another at the magnetopause, there are often instances when one spacecraft exits the magnetopause reconnection layers but another spacecraft does not. Based on these multiple crossings by several spacecraft, it was concluded, for example, that reconnection was continuous for over 2 hours at the magnetopause (although its rate could have been modulated) (Phan et al. 2004).

The temporal character of reconnection with and without a guide field (i.e., of component vs. antiparallel reconnection) has been studied in PIC simulations by Drake et al. (2006), who found that, once initiated, antiparallel reconnection remains steady. In contrast, in the presence of a guide field, the current layer grows and becomes unstable to the formation of magnetic islands, producing a bursty outflow of ions. Kinetic simulations by Karimabadi et al. (2007) with no guide field indicate that reconnection can occur in a quasi-steady fashion, owing to a balance between the outward convection of the magnetic field and the electron pressure; ultimately, however, the electron current sheet elongates, resulting in the formation of secondary islands and greater variability in the reconnection rate. Formation of secondary islands during magnetopause reconnection formation is a possible explanation for the occurrence of FTEs (Drake et al. 2006; Karimabadi et al. 2007). Evidence of secondary island formation is sparse. However, magnetic islands have been observed during reconnection events in the tail, both in the presence of a guide field (Eastwood et al. 2007) and without a guide field (Chen 2009). Teh et al. (2010) report a secondary island during a nearly antiparallel reconnection event at the magnetopause.

The basic difficulty in determining reconnection rates at the magnetopause (either absolute rates or relative rates) is that ion and electron features (e.g., reconnection jets) observed by spacecraft outside the electron diffusion region are essentially independent of the reconnection rate. In addition, it was demonstrated in Sect. 5.1 that the rate is difficult to measure and, for spacecraft at the magnetopause, there are no successive measurements of the rate on 1–2 minute timescales (i.e., commensurate with predicted variability) that could be used to demonstrate that magnetopause reconnection rates are variable.

To search for reconnection rate variability, researchers have turned to the magnetospheric cusps. Spacecraft traversing the cusp at low altitudes observe an ion dispersion where, for southward IMF, highest energy magnetosheath ions are observed at low latitudes and successively lower energy ions are observed at successively higher latitudes. The reverse dispersion is observed for northward IMF. This same dispersion was discussed in Sect. 4 in conjunction with the distance to the reconnection line. This energy-latitude ion dispersion is consistent with dayside magnetic reconnection either at low latitudes for southward IMF or high latitudes poleward of the cusp for northward IMF.

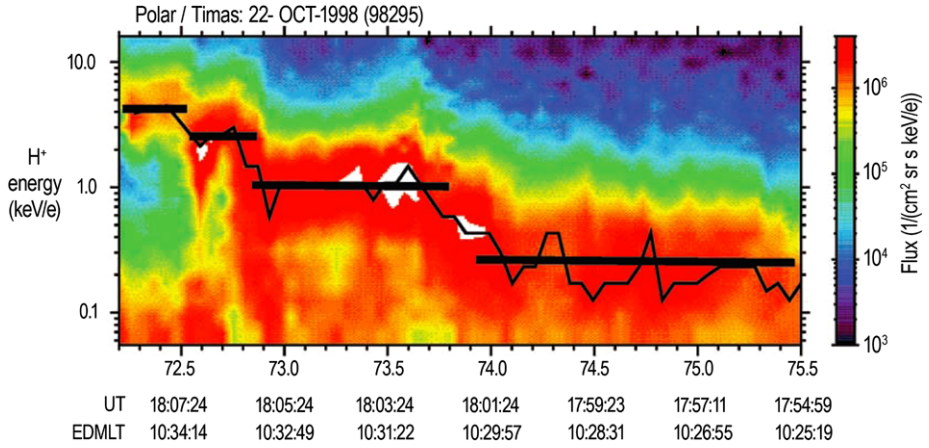

Fig. 10 Ion fluxes in the cusp for southward IMF conditions. The energy of maximum flux decreases in four distinct steps from low to high latitude. These steps have been interpreted as evidence for spatial processes in the cusp and also evidence for variability in the reconnection rate at the magnetopause. From Trattner et al. (2002b)

For reconnection that is spatially and temporally independent, a spacecraft would observe a smooth energy-latitude dispersion as it traverses the cusp. Such a smooth dispersion is rarely seen. Figure 10 shows a typical energy-latitude dispersion example observed in the cusp for southward IMF (from Trattner et al. 2002a).

Figure 10 is an energy-latitude spectrogram of the proton flux in the cusp. The spacecraft actually traversed the cusp from high to low latitude, so time is plotted in reverse. The energy of the peak flux (identified by the thin black line) decreases from low to high latitude as expected; however, the decrease is not smooth. A series of four distinct steps occur where the energy of the peak flux decreases rapidly and then remains nearly constant for much longer periods of time. The thick black lines were added to the figure to emphasize these four steps. Within these steps, the energy of maximum flux shows considerable variability.

Steps in ion dispersions in the cusp are interpreted as spatial changes in the cusp or temporal changes in the reconnection rate (or some combination of both types of changes). The spatial interpretation uses the fact that a spacecraft does not follow a single flux tube as it traverses the cusp in both latitude and longitude. Therefore, it is possible to cross flux tubes that have different time histories since their reconnection at the dayside magnetopause. As a result, even for a time-independent reconnection rate at the magnetopause, steps occur in the cusp as the spacecraft transitions from one flux tube to another.

Alternatively, the reconnection rate could be time dependent. Rapid changes in the energy of the peak flux indicate times when reconnection was active and constant energy times represent times when the reconnection rate was very small or zero (Lockwood and Smith 1992).

Multi-spacecraft observations and combination with ground-based observations of ionospheric flow are used to distinguish spatial from temporal effects (e.g., Onsager et al. 1995; Trattner et al. 2002b, 2003). Basically, if the same steps in the energy of the peak flux are observed at the same latitude by a spacecraft that traverses the cusp sometime after the first spacecraft, then the steps are spatial in nature. Indeed, the cusp crossing in Fig. 10 was followed by a second spacecraft crossing, which observed the same four steps (Trattner et al.

2002a). Thus, for this event, the steps have a spatial origin and one can conclude that the observations are consistent with steady (or at least quasi-steady) reconnection.

Conversely, if two spacecraft observe steps displaced in latitude at different times, then these steps represent time dependent reconnection. There are certainly many examples of temporal cusp features that are consistent with variable reconnection (e.g., Trattner et al. 2003).

Tests used to distinguish temporal or spatial origin of cusp ion dispersion steps require two or more spacecraft in the cusp either simultaneously or within a short time of one another and often observations of convection patterns in the ionosphere are needed also to help with this distinction. Combined multi-spacecraft and ground-based observations in the cusp are not made frequently and, thus far, only event studies have been performed. Thus, there is currently no statistical study that determines how variable reconnection rates are at the magnetopause and under what external conditions this variability dominates.

6 Future Reconnection Observations: The Magnetospheric Multiscale (MMS) Mission

In the near future, the MMS mission will make new observations of magnetic reconnection at the magnetopause and in the magnetotail (Burch and Drake 2009). The overarching goal of the MMS mission is to measure ion and electron distributions and electric and magnetic fields inside the electron and ion diffusion regions in the Earth's magnetosphere to answer the following fundamental questions:

(1) What conditions determine when reconnection is initiated and when it ceases?
(2) What determines the rate at which reconnection occurs?
(3) What are the structures and dimensions of the electron and ion diffusion regions?
(4) How do the plasma and magnetic field become decoupled in the electron diffusion region? In particular, what role do electrons play in facilitating reconnection?
(5) What is the role of turbulence in the reconnection process?
(6) How does reconnection accelerate particles to high energies?

The mission consists of four spacecraft carrying identical suites of plasma and field instruments. An important advance in reconnection observations is that these instruments will measure ion and electron distributions and electric and magnetic fields with unprecedented high (millisecond) time resolution and accuracy. The spacecraft will fly in a tetrahedral (pyramid) formation allowing them to determine three dimensional structures of reconnection sites they encounter. Onboard propulsion adjusts spacecraft separation. Optimal separation will be determined during the mission, but separations as small as 10 km are possible and planned.

On board propulsion will also be used to make significant changes in the orbits of the spacecraft. The tetrahedral formation starts out (in mission phase 1) in a 1.2×12 R_E elliptical orbit that allows exploration of reconnection sites near the dayside equatorial region. After this first mission phase, propulsion is used to increase the apogee so that the tetrahedral formation is in a 1.2×25 R_E orbit that cuts through the magnetotail region where nightside, near-Earth reconnection sites are formed. This mission draws on 30+ years of theoretical and observational reconnection research that has culminated in the exploration of the ion diffusion region and determined relevant scale lengths for phenomena associated with the electron diffusion region. In the next section, Sects. 3 through 5 of this paper are reviewed with emphasis on the implications for this new and ambitious mission.

7 Discussion and Conclusions

Theory and modeling have established scale lengths of important phenomena associated with reconnection. In Sect. 3, some of the important scale lengths were reviewed and Fig. 2 summarizes many of these scale lengths. For the most part, ion scale lengths have been confirmed using single and multi-spacecraft observations in the magnetotail and at the magnetopause. Observations have confirmed the existence of out-of-plane Hall fields and have demonstrated that the quadrupolar Hall fields become bi-polar for asymmetric reconnection at the magnetopause (Mozer et al. 2008a, 2008b). Although Fig. 2 shows that out-of-plane Hall fields occur in the ion diffusion region (where the ions are demagnetized), there is also theoretical and observational evidence that these fields extend far beyond the traditional diffusion region dimensions, especially along the separatrices. Thus, using these fields to determine the width of the ion diffusion region would result in a significant overestimate of this dimension. This complication in the width of the ion diffusion region aside, overall dimensions of the ion diffusion region have been confirmed using a variety of spacecraft observations. In particular, the thickness of the diffusion region has been shown to be of the order of an ion skin depth, as illustrated in Fig. 2.

Reconnection features associated with the electron diffusion region have also been identified in spacecraft data. Time resolution of current particle instrumentation precludes investigating characteristics of electrons in these reconnection features. However, electric and magnetic field observations and partial measurements of electron distributions in these features confirm their existence. In particular, high energy electrons are found in narrow layers associated with the separatices extending from the reconnection region.

These scale length estimates for reconnection regions have important implications for future spacecraft missions like MMS. In most simulations, the dimensions of the ion and electron diffusion regions are related by the absolute quantity, $\sqrt{m_i/m_e}$. Therefore, combined observations that verify theoretical estimates of ion diffusion region dimensions also indicate that electron diffusion region dimensions are as predicted by current reconnection theory. The time resolution requirements for the electron measurements for the MMS mission were determined from these theoretical estimates of the electron diffusion region dimensions. Therefore, scale length determinations of the ion diffusion region dimensions provide confidence that electron measurement requirements are sufficient for answering MMS mission science questions.

The observation of electron scale length features associated with reconnection separatrices (André et al. 2004) also suggests an important opportunity for the MMS mission. Electrons traveling along the separatrices originate in or very near the electron diffusion region. Therefore, properties of these electrons may provide important insight into the diffusion region even though a spacecraft may not pass directly through the very small region. To be sure, these properties are greatly modified by the intense wave-particle interactions that occur in association with the electron beams (Drake et al. 2003; Cattell et al. 2005). However, detailed measurements of the plasma properties of the beams and high resolution electric and magnetic field measurements from MMS, when combined with computer simulations, hold the promise to untangle the wave-particle effects and determine the properties of electrons that exit the diffusion region.

Recent studies of magnetic reconnection have also provided important information on the location of reconnection and the type of reconnection (guide field or anti-parallel). In the magnetotail, it is often assumed that reconnection occurs between anti-parallel fields. However, in the distant tail reconnection event in Fig. 5 (from Øieroset et al. 2001), the non-zero B_y component is consistent with component (or guide field) reconnection. Recent case

studies (e.g., Nakamura et al. 2008) and a limited statistical study (Eastwood et al. 2010) indicate that guide field reconnection is relatively common in the near-tail as well. Thus, reconnection geometries in the tail may be considerably more complex than previously assumed.

There is ample evidence of both anti-parallel and component reconnection at the dayside magnetopause. Recently, Trattner et al. (2007a, 2007b) used 130 traversals of the Earth's magnetospheric cusps under a variety of IMF conditions to determine when and where anti-parallel and component reconnection occur at the magnetopause. For southward IMF, anti-parallel reconnection occurs when B_x is much larger than B and when $|B_z|$ is larger than $|B_y|$. Component reconnection occurs when $|B_y|$ is larger than $|B_z|$. Anti-parallel reconnection occurs at relatively high latitudes while component reconnection occurs at lower latitudes and with relatively high frequency near the subsolar region (although where the reconnection line crosses the noon meridian is seasonally dependent). On the flanks of the magnetopause, reconnection is predominantly anti-parallel.

These results have important implications for MMS mission planning. Because of spacecraft fuel constraints, the first phase of the mission is confined to lower latitudes at the dayside magnetopause. This constraint can be turned into an advantage by using careful orbit planning and the known occurrence frequency of component reconnection to maximize the probability of encountering the reconnection diffusion region (Griffiths et al. 2011). The recent work on reconnection topology also indicates that the MMS spacecraft will encounter component or guide field reconnection most often at the dayside magnetopause. However, encounters of anti-parallel reconnection are possible on the flanks of the magnetopause, on the dayside when $|B_z|$ is very large compared to $|B|$, and in the magnetotail.

Reconnection rates in the near-Earth magnetotail (between 20 and 30 R_E from the Earth on the nightside) are highly variable. A typical substorm cycle is about 3 hours, during which a near-Earth reconnection line might exist for less than one third of the time. Thus, measurements inside a near-Earth reconnection line by MMS will require significant dwell time in the vicinity of the Earth's neutral sheet. The MMS orbit is designed to pass through the magnetotail at nearly zero ecliptic inclination, maximizing the dwell time near the neutral sheet.

Reconnection rates at the dayside magnetopause range from 0.01 to greater than 0.1 (using V_n/V_A as a proxy for the reconnection rate). These rates may be highly variable or may be quite stable. Thus far, the interpretation of FTEs at the magnetopause provides the best evidence of variable reconnection at the magnetopause. However, this evidence and other evidence from the magnetospheric cusps do not demonstrate conclusively that reconnection ever goes to zero at the magnetopause.

The ratio of the thickness to the width of the electron (or ion) diffusion region is proportional to the reconnection rate. If the electron diffusion region is a few kilometers thick (as illustrated in Fig. 2), then reconnection rates (in Fig. 9) higher than 0.1 suggest that there are times when the width of the diffusion region is less than ~20 km. Similarly, the large number of rates significantly below 0.1 suggests that the diffusion region width could be significantly greater than 20 km, perhaps even as large as 200 km. Simulations and recent Cluster observations (Phan et al. 2007; Chen 2009) indicate that the electron diffusion region can extend to 10s of ion skin depths from the x-line. As discussed above, the elongated diffusion region consists of an inner region and extended collimated outflow jet. Klimas et al. (2008) have demonstrated that it is only the aspect ratio of the inner region that is related to the reconnection rate and propose that the term "electron diffusion region" be used only with reference to this inner region, which in other simulations (Karimabadi et al. 2007; Shay et al. 2007) appears to be a few ion skin depths in extent rather than a few electron skin

depths. Although this seems like a significant increase in the diffusion region dimensions, the region is still very small compared to the overall surface area of the magnetopause. Thus, the probability of encountering this small region by the MMS spacecraft remains at most a few percent (Griffiths et al. 2011).

In summary, recent spacecraft observations have confirmed several theoretical predictions and indicated some new features of ion and electron diffusion regions. They also set the stage for the next significant advancement of the understanding of reconnection gleaned from the future MMS mission.

Acknowledgements The authors thank Tai Phan and Marit Øieroset for their comments on this manuscript.

References

M. André et al., Thin electron-scale layers at the magnetopause. Geophys. Res. Lett. 31 (2004). doi:10.1029/2003GL018137

S.V. Badman, S.W.H. Cowley, Significance of Dungey-cycle flows in Jupiter's and Saturn's magnetospheres and their identification on closed equatorial field lines. Ann. Geophys. (2007). doi:10.5194/angeo-25-941-2007

A. Balogh et al., The cluster magnetic field investigation: scientific objectives and instrumentation, ESA SP-1159, 95 (1993)

W. Baumjohann, The near Earth plasma sheet—an AMPTE/IRM perspective. Space Sci. Rev. **64**, 141 (1993)

A.L. Borg et al., Cluster encounter of a magnetic reconnection diffusion region in the near-Earth magnetotail on September 19, 2003. Geophys. Res. Lett. (2005). doi:10.1029/2005GL023794

J.L. Burch, J.F. Drake, Reconnecting magnetic fields. Am. Sci. **97**, 392 (2009)

P.A. Cassak, M.A. Shay, Scaling of asymmetric magnetic reconnection: General theory and collisional simulations. Phys. Plasmas **14**, 102114 (2007)

P.A. Cassak, M.A. Shay, Scaling of asymmetric Hall magnetic reconnection. Geophys. Res. Lett. (2008). doi:10.1029/2008GL035268

C. Cattell et al., Cluster observations of electron holes in association with magnetotail reconnection and comparison to simulations. J. Geophys. Res. (2005). doi:10.1029/2004JA010519

L.-J. Chen, Multispacecraft observations of the electron current sheet, neighboring magnetic islands, and electron acceleration during magnetotail reconnection. Phys. Plasmas (2009). doi:10.1063/1.3112744

W. Daughton, J. Scudder, H. Karimabadi, Fully kinetic simulations of undriven magnetic reconnection with open boundary conditions. Phys. Plasmas (2006). doi:10.1063/1.2218817

F. deHoffmann, E. Teller, Magneto-hydrodynamic shocks. Phys. Rev. **80**, 692 (1950)

X.H. Deng et al., Geotail encounter with reconnection diffusion region in the Earth's magnetotial: Evidence of multiple X lines collisionless reconnection? J. Geophys. Res. (2004). doi:10.1029/2003JA010031

J.F. Drake et al., Formation of electron holes and particle energization during magnetic reconnection. Science **299**, 873 (2003)

J.F. Drake, M. Swisdak, K.M. Schoeffler, B.N. Rogers, S. Kobayashi, Formation of secondary islands during magnetic reconnection. Geophys. Res. Lett. (2006). doi:10.1029/2006GL025957

J.F. Drake, M.A. Shay, M. Swisdak, The Hall fields and fast magnetic reconnection. Phys. Plasmas **15** (2008). doi:10.1063/1.2900194

J.F. Drake et al., Ion heating resulting from pickup in magnetic reconnection exhausts. J. Geophys. Res. (2009). doi:10.1029/2008JA013701

J.W. Dungey, Conditions for the occurrence of electrical discharges in astrophysical systems. Philos. Mag. **44**, 725 (1953)

J.W. Dungey, Interplanetary magnetic field and the auroral zones. Phys. Rev. Lett. **6**, 47 (1961)

J.P. Eastwood et al., Multi-point observations of the Hall electromagnetic field and secondary island formation during magnetic reconnection. J. Geophys. Res. (2007). doi:10.1029/2006JA012158

J.P. Eastwood, T.D. Phan, M. Øieroset, M.A. Shay, Average properties of the magnetic ion diffusion region in the Earth's magnetotail: The 2001–2005 Cluster observations and comparison with simulations. J. Geophys. Res. (2010). doi:10.1029/2009JA014962

L.A. Frank, K.L. Ackerson, R.P. Lepping, Hot tenuous plasmas, fireballs, and boundary layers in the Earth's magnetotail. J. Geophys. Res. (1976). doi:10.1029/JA081i034p05859

M. Fujimoto et al., Observations of earthward streaming electrons at the trailing boundary of a plasmoid. Geophys. Res. Lett. **24**, 2893 (1997)

S.A. Fuselier, H.U. Frey, K.J. Trattner, S.B. Mende, J.L. Burch, Cusp aurora dependence on interplanetary magnetic field B_z. J. Geophys. Res. (2002). doi:10.1029/2001JA900165
S.A. Fuselier, K.J. Trattner, S.M. Petrinec, C.J. Owen, H. Rème, Computing the reconnection rate at the Earth's magnetopause using two spacecraft observations. J. Geophys. Res. (2005). doi:10.1029/2004JA010805
S.A. Fuselier, S.M. Petrinec, K.J. Trattner, Anti-parallel magnetic reconnection rates at the Earth's magnetopause. J. Geophys. Res. (2010). doi:10.1029/2010JA015302
J.T. Gosling, R.M. Skoug, D.J. McComas, C.W. Smith, Direct evidence for magnetic reconnection in the solar wind near 1 AU. J. Geophys. Res. (2005). doi:10.1029/2004JA010809
J.T. Gosling, S. Eriksson, R.M. Skoug, D.J. McComas, R.J. Forsyth, Petschek-type magnetic reconnection exhausts in the solar wind well beyond 1 AU: Ulysses. Astrophys. J. (2006a). doi:10.1086/503544
J.T. Gosling, S. Eriksson, R. Schwenn, Petschek-type magnetic reconnection exhausts in the solar wind well inside 1 AU: Helios. J. Geophys. Res. (2006b). doi:10.1029/2006JA011863
S.T. Griffiths et al., A probability assessment of encountering dayside magnetopause diffusion regions. J. Geophys. Res. (2011). doi:10.1029/2010JA015136
G. Gustafsson et al., The spherical probe electric field and wave experiment for Cluster, ESA SP-1159, 17 (1993)
S.E. Haaland et al., Four-spacecraft determination of magnetopause orientation, motion, and thickness: comparison with results from single-spacecraft methods. Ann. Geophys. **22**, 1347 (2004)
M. Hesse, Dissipation in magnetic reconnection with a guide magnetic field. Phys. Plasmas **13**, 1220107 (2006)
M. Hesse, J. Birn, M. Kuznetsova, Collisionless magnetic reconnection: Electron processes and transport modeling. J. Geophys. Res. **196**, 3721 (2001)
M. Hesse, M. Kuznetsova, J. Birn, The role of electron heat flux in guide-field magnetic reconnection. Phys. Plasmas **11**, 125387 (2004)
E.W. Hones Jr., Observations in the Earth's magnetotail relating to magnetic merging. Sol. Phys. (1976). doi:10.1007/BF00152248
E. Hones (ed.), *Magnetic Reconnection in Space and Laboratory Plasmas*. Geophysical Monograph, vol. 30 (American Geophysical Union, Washington DC, 1984)
B. Hultqvist, M. Øieroset (eds.), *Transport Across the Boundaries of the Magnetosphere* (Kluwer, Dordrecht, 1997). Reprinted from Space Science Reviews, vol. 80, nos. 1–2 (1997)
B. Hultqvist et al. (eds.), *Magnetospheric Plasma Sources and Losses* (Kluwer Academic, Dordrecht, 1999). Reprinted from Space Sci. Rev., vol. 88, nos. 1–2 (1999)
C.M. Jackman et al., A multi-instrument view of tail reconnection at Saturn. J. Geophys. Res. (2008). doi:10.1029/2008JA013592
H. Karimabadi, W. Daughton, J. Scudder, Multi-scale structure of the electron diffusion region. Geophys. Res. Lett. (2007). doi:10.1029/2007GL030306
M.G. Kivelson, D.J. Southwood, Dynamical consequences of two modes of centrifugal instability in Jupiter's outer magnetosphere. J. Geophys. Res. (2005). doi:10.1029/2005JA011176
A. Klimas, M. Hesse, S. Zenitani, Particle-in-cell simulations of collisionless reconnection with open outflow boundaries. Phys. Plasmas (2008). doi:10.1063/1.2965826
E.A. Kronberg, J. Woch, N. Krupp, A. Lagg, K.K. Khurana, K.-H. Glassmeier, Mass release at Jupiter: Substorm-like processes in the Jovian magnetotail. J. Geophys. Res. (2005). doi:10.1029/2004JA010777
R.H. Levy, H.E. Petschek, G.L. Siscoe, Aerodynamic aspects of the magnetospheric flow. AIAA J. **2**, 2065 (1964)
M. Lockwood, M.F. Smith, The variation of reconnection rate at the dayside magnetopause and cusp ion precipitation. J. Geophys. Res. **97**, 14841 (1992)
M. Manapat et al., Field-aligned electrons at the lobe/plasma sheet boundary in the mid-to-distant magnetotail and their association with reconnection. Geophys. Res. Lett. (2006). doi:10.1029/2005GL024971
H.J. McAndrews et al., Evidence of reconnection at Saturn's magnetosphere. J. Geophys. Res. (2008). doi:10.1029/2007JA012581
F.S. Mozer, Criteria for and statistics of electron diffusion regions associated with subsolar magnetic field reconnection. J. Geophys. Res. (2005). doi:10.1029/2005JA011258
F.S. Mozer, A. Hull, Scaling the energy conversion rate from magnetic field reconnection to different bodies. Phys. Plasmas **17**, 102906 (2010)
F.S. Mozer, P.L. Pritchett, Electron physics of asymmetric magnetic field reconnection. Space Sci. Rev. (2011). doi:10.1007/s11214-010-9681-8
F.S. Mozer, A. Retinò, Quantitative estimates of magnetic field reconnection properties from electric and magnetic field measurements. J. Geophys. Res. (2007). doi:10.1029/2007JA012406

F.S. Mozer, S.D. Bale, T.D. Phan, Observations of ion and electron diffusion regions at a sub-solar magnetopause reconnection event. Phys. Rev. Lett. **89**, 015002 (2002)
F.S. Mozer, S.D. Bale, T.D. Phan, J.A. Osborne, Observations of electron diffusion regions at the subsolar magnetopause. Phys. Rev. Lett. (2003). doi:10.1103/PhysRevLett.91.245002 015002
F.S. Mozer, V. Angelopoulos, J. Bonnell, K.H. Glassmeier, J.P. McFadden, THEMIS observations of modified Hall fields in asymmetric magnetic field reconnection. Geophys. Res. Lett. (2008a). doi:10.1029/2007GL033033
F.S. Mozer, P.L. Pritchett, J. Bonnell, D. Sundkvist, M.T. Chang, Observations and simulations of asymmetric magnetic field reconnection. J. Geophys. Res. (2008b). doi:10.1029/2008JA013535
T. Nagai, Location of magnetic reconnection in the magnetotail. Space Sci. Rev. (2006). doi:10.1107/s11214-006-6216-4
T. Nagai et al., Geotail observations of the Hall current system: Evidence of magnetic reconnection in the magnetotail. J. Geophys. Res. **106**, 25929 (2001)
T. Nagai et al., Structure of the Hall current system in the vicinity of the magnetic reconnection site. J. Geophys. Res. (2003). doi:10.1029/2003JA009900
T. Nagai et al., Construction of magnetic reconnection in the near-Earth magnetotail with Geotail. J. Geophys. Res. (2010). doi:10.1029/2010JA016283
R. Nakamura et al., Cluster observations of an ion-scale current sheet in the magnetotail under the presence of a guide field. J. Geophys. Res. (2008). doi:10.1029/2007JA012760
M. Øieroset et al., In situ detection of collisionless reconnection in the Earth's magnetotail. Nature **412**, 414 (2001)
T.G. Onsager, M.F. Thomsen, R.C. Elphic, J.T. Gosling, Model of electron and ion distributions in the plasma sheet boundary layer. J. Geophys. Res. **96**, 20999 (1991)
T.G. Onsager et al., Low-altitude observations and modeling of quasi-steady magnetopause reconnection. J. Geophys. Res. **100**, 11831 (1995)
C.J. Owen et al., Cluster observations of "crater" flux transfer events at the dayside high-latitude magnetopause. J. Geophys. Res. (2008). doi:10.1029/2007JA012701
E.N. Parker, The solar flare phenomenon and the theory of reconnection and annihilation of magnetic fields. Astron. Astrophys. Suppl. Ser. **8**, 177 (1963)
G. Paschmann, Recent in situ observations of magnetic reconnection in near-Earth space. Geophys. Res. Lett. (2008). doi:10.1029/2008GL035297
G. Paschmann et al., Plasma acceleration at the Earth's magnetopause: Evidence for reconnection. Nature (1979). doi:10.1038/282243a0
S.M. Petrinec, S.A. Fuselier, On continuous versus discontinuous neutral lines at the dayside magnetopause for southward interplanetary magnetic field. Geophys. Res. Lett. 1519 (2003). doi:10.1029/2002GL016565
H.E. Petschek, Magnetic field annihilation, in *The Physics of Solar Flares*, ed. by W.N. Hess (NASA, Washington DC, 1964), p. 425
T.-D. Phan, G. Paschmann, Low-latitude dayside magnetopause and boundary layer for high magnetic shear 1. Structure and motion. J. Geophys. Res. **101**, 7801 (1996)
T.-D. Phan et al., Extended magnetic reconnection at the Earth's magnetopause from detection of bi-directional jets. Nature **404**, 848 (2000)
T.-D. Phan, B.U.Ö. Sonnerup, R.P. Lin, Fluid and kinetics signatures of reconnection at the dawn tail magnetopause: Wind observations. J. Geophys. Res. **106**, 25489 (2001)
T.-D. Phan et al., Simultaenous Cluster and IMAGE observations of cusp reconnection and auroral proton spot for northward IMF. Geophys. Res. Lett. (2003). doi:10.1029/2003GL016885
T.D. Phan et al., Cluster observations of continuous reconnection at the magnetopause under steady interplanetary magnetic field conditions. Ann. Geophys. **22**, 2355 (2004)
T.D. Phan et al., A magnetic reconnection X-line extending more than 390 Earth radii in the solar wind. Nature (2006). doi:10.1038/nature04393
T.-D. Phan et al., Evidence for an elongated (>60 ion skin depths) electron diffusion region during fast magnetic reconnection. Phys. Rev. Lett. (2007). doi:10.1103/PhysRevLett.99255002
P.L. Pritchett, Geospace environment modeling magnetic reconnection challenge: Simulations with a full particle electromagnetic code. J. Geophys. Res. **106**, 3793 (2001)
A. Retinò et al., Cluster multispacecraft observations at the high-latitude duskside magnetopause: implications for continuous and component magnetic reconnection. Ann. Geophys. **23**, 461 (2005)
A. Runov et al., Current sheet structure near magnetic X-line observed by Cluster. Geophys. Res. Lett. (2003). doi:10.1029/2002GL016730
C.T. Russell, R.C. Elphic, Initial ISEE magnetometer results: Magnetopause observations. Space Sci. Rev. **22**, 681 (1978)

C.T. Russell, R.C. Elphic, ISEE observations of flux transfer events at the dayside magnetopause. Geophys. Res. Lett. **6**, 33 (1979)
C.T. Russell, R.J. Walker, Flux transfer events at Mercury. J. Geophys. Res. **90**, 11067 (1985) (1985)
C.T. Russell, K.K. Khurana, D.E. Huddleston, M.G. Kivelson, Localized reconnection in the near Jovian magnetotail. Science (1988). doi:10.1126/science.280.5366.1061
M. Scholer, Magnetic flux transfer at the magnetopause based on single X-line bursty reconnection. Geophys. Res. Lett. **15**, 291 (1988)
J.D. Scudder, F.S. Mozer, N.C. Maynard, C.T. Russell, Fingerprints of collisionless reconnection at the separator. I. Ambipolar Hall signatures. J. Geophys. Res. (2002). doi:10.1029/2001JA000126
M.A. Shay, J.F. Drake, B.N. Rogers, R.E. Denton, The scaling of collisionless, magnetic reconnection for large systems. Geophys. Res. Lett. (1999). doi:10.1029/1999GL900481
M.A. Shay, J.F. Drake, M. Swisdak, Two-scale structure of the electron dissipation region during collisionless magnetic reconnection. Phys. Rev. Lett. (2007). doi:10.1103/PhysRevLett.99.155002
J.A. Slavin et al., MESSENGER observations of magnetic reconnection in Mercury's magnetosphere. Science (2009). doi:10.1126/science.1172011
P. Song, B.U.Ö. Sonnerup, M.F. Thomsen (eds.), *Physics of the Magnetopause*, Geophysical Monograph, vol. 90 (American Geophysical Union, Washington DC, 1995)
B.U.Ö. Sonnerup, Magnetic field reconnection, in *Solar System Plasma Physics III*, ed. by L.T. Lanzertotti, C.F. Kennel, E.N. Parker (North-Holland, New York, 1979), p. 45
B.U.Ö. Sonnerup, L.J. Cahill Jr., Magnetopause stricter and attitude from Explorer 12 observations. J. Geophys. Res. **72**, 171 (1967)
B.U.Ö. Sonnerup et al., Evidence for magnetic field reconnection at the Earth's magnetopause. J. Geophys. Res. **86**, 10049 (1981)
D.J. Southwood, C.J. Farrugia, M.A. Saunders, What are flux transfer events? Planet. Space Sci. **36**, 503 (1988)
P.A. Sweet, The neutral point theory of solar flares, in *Electromagnetic Phenomena in Cosmical Physics*, ed. by B. Lehnert (Cambridge University Press, London, 1958), p. 123
M. Swisdak, B.N. Rogers, J.F. Drake, M.A. Shay, Diamagnetic suppression of component magnetic reconnection at the magnetopause. J. Geophys. Res. (2003). doi:10.1029/2002JA009726
W.-L. Teh et al., THEMIS observations of a secondary magnetic island within the Hall electromagnetic field region at the magnetopause. Geophys. Res. Lett. (2010). doi:10.1029/2010GL045056
K.J. Trattner et al., Temporal versus spatial interpretation of cusp ion structures observed by two spacecraft. J. Geophys. Res. (2002a). doi:10.1029/2001JA000181
K.J. Trattner, S.A. Fuselier, W.K. Peterson, C.W. Carlson, Spatial features observed in the cusp under steady solar wind conditions. J. Geophys. Res. (2002b). doi:10.1029/2001JA000262
K.J. Trattner et al., Cusp structures combining multi-spacecraft observations with ground-based observations. Ann. Geophys. **21**, 2031 (2003)
K.J. Trattner, J.S. Mulcock, S.M. Petrinec, S.A. Fuselier, Location of the reconnection line at the magnetopause during southward IMF conditions. Geophys. Res. Lett. (2007a). doi:10.1029/2006GL028397
K.J. Trattner, J.S. Mulcock, S.M. Petrinec, S.A. Fuselier, Probing the boundary between antiparallel and component reconnection during southward interplanetary magnetic field conditions. J. Geophys. Res. (2007b). doi:10.1029/2007012270JA
K.J. Trattner, S.M. Petrinec, S.A. Fuselier, W.K. Petersen, R. Friedel, Cusp energetic ions as tracers for particle transport into the magnetosphere. J. Geophys. Res. (2010). doi:10.1029/2009JA014919
L. Trenchi et al., Occurrence of reconnection jets at the dayside magnetopause, Double Star observations. J. Geophys. Res. (2008). doi:10.1029/2007JA012774
A. Vaivads, A. Retinò, M. André, Microphysics of magnetic reconnection. Space Sci. Rev. (2006). doi:10.1007/s11214-006-7019-3
A. Vaivads et al., Structure of the magnetic reconnection diffusion region from four-spacecraft observations. Phys. Rev. Lett. (2004). doi:10.1103/PhysRevLett.93.105001
V.M. Vasyliunas, Theoretical models of magnetic field line merging. Rev. Geophys. (1975). doi:10.1029/RG013i001p00303
M.F. Vogt et al., Reconnection and flows in the Jovian magnetotail as inferred from magnetometer observations. J. Geophys. Res. (2010). doi:10.1029/2009JA015098
H. Zhang et al., Cluster observations of collisionless Hall reconnection at high-latitude magnetopause. J. Geophys. Res. (2008). doi:10.1029/2007JA012789